Journal of Geophysical Research: Oceans

RESEARCH ARTICLE
10.1029/2017JC013697

Reassessing Sea Ice Drift and Its Relationship to Long-Term Arctic Sea Ice Loss in Coupled Climate Models

Neil F. Tandon[1,2], Paul J. Kushner[1], David Docquier[3], Justin J. Wettstein[4,5,6], and Camille Li[5,6]

[1]Department of Physics, University of Toronto, Toronto, ON, Canada, [2]Now at Climate Research Division, Environment and Climate Change Canada, Toronto, ON, Canada, [3]Earth and Life Institute, Université Catholique de Louvain, Louvain-la-Neuve, Belgium, [4]College of Earth, Ocean, and Atmospheric Sciences, Oregon State University, Corvallis, OR, USA, [5]Geophysical Institute, University of Bergen, Bergen, Norway, [6]Bjerknes Centre for Climate Research, Bergen, Norway

Key Points:
- Sea ice drift in climate models is more realistic than previously suggested
- Most models produce realistic long-term increases in winter Arctic average sea ice drift speed
- Most models produce long-term decreases of summer Arctic average drift speed, in poor agreement with observations

Correspondence to:
N. F. Tandon,
neil.tandon@canada.ca

Citation:
Tandon, N. F., Kushner, P. J., Docquier, D., Wettstein, J. J., & Li, C. (2018). Reassessing sea ice drift and its relationship to long-term Arctic sea ice loss in coupled climate models. *Journal of Geophysical Research: Oceans*, *123*, 4338–4359. https://doi.org/10.1029/2017JC013697

Received 11 DEC 2017
Accepted 26 APR 2018
Accepted article online 4 MAY 2018
Published online 30 JUN 2018

Abstract Results of an earlier study suggest that sea ice drift in climate models is unrealistic, and this has undermined confidence in model projections of "long-term" (i.e., secular) Arctic sea ice loss. We revisit this by analyzing 22 models participating in phase 5 of the Coupled Model Intercomparison Project (CMIP5). It is shown that, when consistent temporal sampling is applied, sea ice drift speed in models and observations come into closer agreement than previously suggested. There is still considerable intermodel scatter in climatological drift speed, and we show that much of this likely relates to prescribed parameters in the sea ice models. Since 1979, observations show a long-term positive trend of annual mean Arctic average sea ice drift speed resulting primarily from sea ice thinning, and most of the CMIP5 models qualitatively reproduce this. The simulated annual mean drift speed trends reflect strong cancellation between winter trends (which are positive in most models and in good agreement with observations) and summer trends (which are negative in most models and in poor agreement with observations). Positive Arctic average drift speed trends do not consistently coincide with positive trends of Fram Strait outflow. The simulated regional relationship between sea ice strength and drift speed changes dramatically as the Arctic transitions from full to partial ice cover, and this "sea ice extent effect" likely influences simulated summer drift speed trends. Altogether, these results highlight aspects in which models show encouraging agreement with observations, while pinpointing aspects in which models require improvement.

1. Introduction

Arctic sea ice extent has exhibited clear negative trends since 1979 (Serreze et al., 2007; Stroeve et al., 2012a), and these negative trends are especially strong during the summer (e.g., Comiso et al., 2008; Stroeve et al., 2012a; Wang & Overland, 2009). This raises the urgency of understanding the physical processes driving "long-term" (i.e., secular) Arctic sea ice loss. Climate model projections are important tools for anticipating and understanding such changes, but there is great concern that climate models are underpredicting the rates of sea ice area and volume loss (Notz & Stroeve, 2016; Stroeve et al., 2007, 2012b; Winton, 2011). Various model deficiencies have been proposed as being responsible for this, including poor representation of melt ponds and ice albedo (Holland et al., 2012; Stroeve & Notz, 2015), poor representation of Arctic clouds (Gorodetskaya et al., 2008) and ocean heat fluxes (Maslowski et al., 2004), and underestimation of incoming longwave radiation (Notz & Stroeve, 2016).

Changes in sea ice drift might also affect the rate of sea ice loss. Atmospheric winds are a key driver of sea ice motion, and numerous studies have suggested that changes in the atmospheric circulation act to accelerate the rate of sea ice loss. In particular, it has been proposed that changes in the atmospheric circulation lead to increased export of sea ice through Fram Strait (Langehaug et al., 2013; Rampal et al., 2011; Smedsrud et al., 2011, 2017; Wettstein & Deser, 2014; Williams et al., 2016). These changes in the atmospheric circulation are in turn connected to large-scale changes in sea level pressure (Deser et al., 2000; Kwok et al., 2004; Rigor et al., 2002; Screen et al., 2011; Serreze et al., 2016; Wettstein & Deser, 2014). Others have argued that the atmospheric circulation influences sea ice loss through changes in downwelling longwave radiation (Ding et al., 2017).

© 2018. The Authors.
This is an open access article under the terms of the Creative Commons Attribution-NonCommercial-NoDerivs License, which permits use and distribution in any medium, provided the original work is properly cited, the use is non-commercial and no modifications or adaptations are made.

Sea ice strength is another important influence on sea ice motion. Earlier studies have shown that as sea ice concentration and thickness decrease, sea ice strength, and internal stress also decrease, leading to more sea ice deformation and fracturing and an increase in drift speed. This connection between sea ice strength and sea ice drift is apparent in both the seasonal cycle and long-term trends (Haas et al., 2008; Olason & Notz, 2014; Rampal et al., 2009).

Building on this, Rampal et al. (2011) have suggested that there is a sea ice "drift acceleration feedback": as ice thins, it becomes more mobile, which leads to additional ice fracturing, more open water and enhanced sea ice melt during summer. Rampal et al. (2011) have performed analysis suggesting that climate models do not capture this positive feedback and that climate models produce sea ice drift speed climatologies that do not agree with observations. These are considered to be fundamental flaws that undermine confidence in the ability of climate models to accurately project Arctic sea ice loss (Notz, 2012; Rampal et al., 2011; Stroeve & Notz, 2015). Complicating matters is the fact that drift acceleration is expected to have the opposite effect on sea ice volume during winter compared to summer: when temperatures are below freezing, more open water formation promotes additional sea ice formation. So it is not at all obvious that sea ice drift acceleration should accelerate long-term sea ice loss.

In this study, we show that sea ice drift in modern climate models is more realistic than previously suggested, and consistent temporal sampling is crucial when comparing model and observed drift speed. Long-term winter trends of sea ice drift speed in most models agree with observations, and these trends are primarily associated with long-term sea ice thinning. However, summer drift speed trends in models are in poor agreement with available observations, and most models show negative trends in summer sea ice drift speed in the mid to late 21st century. This combined with the limited availability of regional summer sea ice drift observations makes it difficult to assess whether drift acceleration will accelerate long-term Arctic sea ice loss. This paper instead focuses on the physical mechanisms in coupled models driving long-term trends in Arctic sea ice drift, with the goal of highlighting aspects in which models perform well and other aspects in which models require improvement.

We begin by detailing our methodology (section 2) and evaluating drift speed in climate models (section 3). Then we examine the physical mechanisms driving simulated long-term trends in sea ice drift speed during winter (section 4) and summer (section 5). We finish with summary and concluding remarks (section 6).

2. Methods

Most of our analysis uses output from 22 models participating in phase 5 of the Coupled Model Intercomparison Project (CMIP5) (Taylor et al., 2012). Details about the models we analyze are provided in Table 1. Simulations covering the historical period up to 2005 are concatenated with output from the high emission "RCP8.5" scenario thereafter. This allows for analysis of simulated sea ice drift during the historical period as well as projected sea ice drift through the end of the 21st century. Unless otherwise noted, our analysis uses daily output of sea ice drift velocity components and near-surface wind velocity components and monthly output of sea ice thickness and sea ice concentration. Below, we provide additional motivation for our specific choices of temporal resolution.

To examine the role of internal variability, we also analyze output from initial condition ensembles. For each of these ensembles, a particular model is run repeatedly with the same prescribed forcings, and only the initial conditions are perturbed. Each run of an ensemble is referred to as an "ensemble member" or "realization." In this study, we examine a four member ensemble of IPSL-CM5A-LR and a five member ensemble of MIROC5.

Most modern climate models implement the elastic-viscous-plastic (EVP) sea ice rheology scheme (Hunke & Dukowicz, 1997), which is a computationally more efficient approximation to the canonical viscous-plastic rheology (Hibler, 1979). One model we analyze (CanESM2) uses the cavitating fluid scheme (Flato & Hibler, 1992), which assumes that sea ice has no resistance to shear or divergence. It is also common for modern sea ice models to implement an ice thickness distribution (ITD) to capture the effects of ice thickness variations at the subgrid scale. Of the models we analyze, only CanESM2 lacks an ITD.

While some modeling centers have developed their own distinct sea ice models, there are three sea ice models that have been adopted by multiple modeling centers. These are the Los Alamos Sea Ice Model (CICE) (Hunke et al., 2015), the Louvain-la-Neuve Sea Ice Model (LIM) (Vancoppenolle et al., 2009), and the

Table 1
Details of Models Analyzed in This Study

Model[a]	Number of runs	Period covered	Rheology scheme[c]	Resolution, grid type[d]
ACCESS1.0 (CICE)	1	1961–2100	EVP	1° tripole
ACCESS1.3 (CICE)	1	1950–2100	EVP	1° tripole
BCC-CSM1.1(m) (SIS)	1	1950–2100	EVP	1° tripole
CanESM2[b]	1	1950–2100	cavitating fluid	1.4° spherical polar
CMCC-CESM (LIM)	1	1950–2100	EVP	1° tripole
CMCC-CM (LIM)	1	1950–2100	EVP	2° tripole
CMCC-CMS (LIM)	1	1950–2100	EVP	2° tripole
FGOALS-g2 (CICE)	1	1950–2100	EVP	1° spherical polar
GFDL-CM3 (SIS)	1	1950–2100	EVP	1° tripole
GFDL-ESM2G (SIS)	1	1950–2100	EVP	1° tripole
GFDL-ESM2M (SIS)	1	1950–2100	EVP	1° tripole
HadGEM2-CC (CICE)	1	1950–2099	EVP	1° spherical polar
HadGEM2-ES (CICE)	1	1950–2100	EVP	1° spherical polar
INM-CM4	1	1950–2100	VP	1° displaced pole
IPSL-CM5A-LR (LIM)	4	1950–2100	EVP	2° tripole
IPSL-CM5A-MR (LIM)	1	1950–2100	EVP	2° tripole
IPSL-CM5B-LR (LIM)	1	1950–2100	EVP	2° tripole
MIROC5	5	r1–3: 1950–2100 r4–5: 1950–2035	EVP	1.4° displaced pole
MIROC-ESM	1	1950–2100	EVP	1.4° spherical polar
MIROC-ESM-CHEM	1	1950–2100	EVP	1.4° spherical polar
MPI-ESM-LR	1	1950–2100	VP	1.5° displaced pole
NorESM1-M (CICE)	1	1950–2100	EVP	1° displaced pole

[a]For models with commonly used sea ice components, the component name is shown in parentheses. See the text for additional details. [b]CanESM2 is the only model we analyze that does not implement an ice thickness distribution (ITD) for the subgrid scale. [c]EVP = elastic-viscous-plastic, VP = viscous-plastic. See the text for additional details. [d]Shown is the approximate resolution with respect to longitude of the model's ocean component. See the text for explanations of grid types.

Sea Ice Simulator (SIS) (Delworth et al., 2006), all of which use EVP rheology. Note that different coupled models use different versions and customizations of these sea ice models, so the information in Table 1 provides only a small glimpse of both the common heritage and distinctions between different climate models.

The ocean components of the models have spatial resolutions that vary between 1° and 2° and use different types of grids. The standard spherical polar grid has a singularity at the north pole (a "pole hole") because the spacing between longitude lines vanishes. One way to resolve this is with a "displaced pole" configuration, in which the grid is stretched and the north pole is relocated to a land mass such as Greenland. Another approach is to adopt a "tripole" grid which has two poles in the Northern Hemisphere, both of which are placed on land.

Table 2 shows additional model parameters that likely play key roles in setting the climatological sea ice drift speed in climate models. Higher air-ice drag, C_{da}, increases the momentum transfer between surface wind and sea ice, thereby increasing drift speed. Higher ice-ocean drag, C_{dw}, opposes this effect and reduces drift speed. One might also expect a higher sea ice strength parameter, P^*, to inhibit sea ice deformation and thereby reduce drift speed (Docquier et al., 2017; Rampal et al., 2011). We will discuss in more detail below the possible influence of these model parameters on simulated climatological drift speed.

Several observational data sets are used to evaluate the CMIP5 models. For computing observed sea ice drift speed, we use daily drift velocity point measurements from the International Arctic Buoy Program (IABP) covering the period 1979–2015, as provided within the archive for the Polar Pathfinder data set (Tschudi et al., 2016). Since the IABP data are point measurements, care is required when comparing to gridded climate model output. For this reason, we adopt a domain covering most of the Arctic Ocean, and we compare domain averages of the IABP measurements to domain averages of climate model output, as we detail further below. IABP data provide sufficient spatial coverage for computing Arctic average drift speed, but the spatial sampling is not sufficient for performing detailed regional analysis.

Table 2
Sea Ice Parameters for the Models Examined in This Study

Model	Arctic average drift speed[f] [km d^{-1}]	Strength parameter (P^*) [kN m^{-2}]	Ice-ocean drag (C_{dw}) [$\times 10^{-3}$]	Roughness length [10^{-4} m]	Air-ice drag (C_{da}) [$\times 10^{-3}$]	Reference[g]
FGOALS-g2	3.6	27.5	5.36		1.20	
MIROC5[a,b]	5.3	20.0	20.0	100	3.52	Komuro et al. (2012)
CMCC-CESM[a]	5.5	25.0	5.00	1.00	1.27	
CMCC-CMS[a]	5.7	25.0	5.00	1.00	1.27	
CMCC-CM[a]	5.8	25.0	5.00	1.00	1.27	
GFDL-CM3[c]	6.2	27.5	3.24	1.00	1.27	Delworth et al. (2006)
GFDL-ESM2M[c]	6.5	27.5	3.24	1.00	1.27	Delworth et al. (2006)
HadGEM2-CC[a]	6.7	20.0	15.0	5.00	1.71	McLaren et al. (2006)
GFDL-ESM2G[c]	6.8	27.5	3.24	1.00	1.27	Delworth et al. (2006)
HadGEM2-ES[a]	7.2	20.0	15.0	5.00	1.71	McLaren et al. (2006)
IPSL-CM5B-LR[a]	7.3	20.0	5.00	20.0	2.32	
NorESM1-M[a,d]	7.4		5.36	5.00	1.71	
BCC-CSM1.1(m)[a]	7.6	27.5	3.24	1.00	1.27	Lu et al. (2013)
IPSL-CM5A-LR[a]	8.2	20.0	5.00	20.0	2.32	
MIROC-ESM[a,b]	8.9	20.0	5.00	100	3.52	
MIROC-ESM-CHEM[a,b]	8.9	20.0	5.00	100	3.52	
ACCESS1.0[a,d]	9.1		5.36	5.00	1.71	Bi et al. (2013)
ACCESS1.3[a,d]	9.5		5.36	5.00	1.71	Bi et al. (2013)
IPSL-CM5A-MR[a]	9.8	20.0	5.00	20.0	2.32	
MPI-ESM-LR[a]	10.0	20.0	4.50	10.0	1.98	
CanESM2[a,e]	10.1	27.5	5.50	2.75	1.52	
INM-CM4	15.3	27.5	5.50		3.00	Yakovlev (2003)

Note. The models are arranged in order of increasing climatological mean Arctic average drift speed.
[a]Air-ice drag in these models varies according to a turbulence parameterization that depends on the roughness length and the near-surface stability. In these models, we compute a nominal air-ice drag coefficient for neutral conditions at 10 m above the surface using the formulation $C_{da}=[\kappa/\ln(z_{10}/z_0)]^2$, where $\kappa=0.41$, $z_{10}=10$ m and z_0 is the roughness length. [b]In these models, the roughness length shown applies when there is snow present on sea ice. When the sea ice is bare, the roughness length is 0.02 m. [c]Air-ice drag in these models depends on the roughness length according to the formulation $C_{da}=[\kappa/\ln(z_{10}/z_0)]^2$, where $\kappa=0.41$, $z_{10}=10$ m and z_0 is the roughness length. [d]Sea ice strength in these models is computed using a parameterization of ice ridging based on Rothrock (1975). These models do not have a P^* parameter like that used in Hibler (1979). [e]Roughness length in this model is proportional to sea ice concentration. The roughness length shown corresponds to 100% sea ice concentration. [f]Arctic average drift speed is the annual mean drift speed averaged over 1979–2005. [g]A blank entry in this column indicates that information was obtained through personal communication with members of the modeling center.

For more detailed regional analysis, we use daily output of satellite-based measurements of summer sea ice drift (Kimura et al., 2013; Sumata et al., 2015), which we refer to as the "Kimura" data. These data are derived from the 18.7 GHz channel of the Advanced Microwave Scanning Radiometer (AMSR) instruments on board the EOS Aqua satellite (covering the period 2003–2011) and the GCOM-W1 satellite (covering 2011 to the present). September 2006–2015 Arctic-average drift speed from the Kimura data is 1.2 km d^{-1} lower than that derived from IABP measurements. This is comparable to the uncertainty estimates of the Kimura data (Sumata et al., 2015), so this difference is likely due to inaccuracies in the Kimura data. IABP measurements sample most of the ice-covered regions of the Arctic Ocean during September 2006–2015, so spatial sampling likely does not explain the difference from the Kimura data.

We do not use satellite data for trend analysis because of the lack of reliable summer data prior to 2003 and because earlier studies have already documented winter trends from satellite observations. In particular, Olason and Notz (2014) show close agreement between satellite and IABP-derived trends of winter Arctic average sea ice drift speed. Furthermore, Spreen et al. (2011) have performed regional analysis of winter drift speed trends from satellite observations. Below we discuss how the results from these studies compare to results from the CMIP5 models.

For observed sea ice concentration, we use the monthly mean Goddard Merged passive microwave measurements provided by the National Snow and Ice Data Center (NSIDC) (Meier et al., 2013). Estimates of observed near-surface wind speed and velocity are obtained from ERA-Interim Reanalysis (Dee et al., 2011).

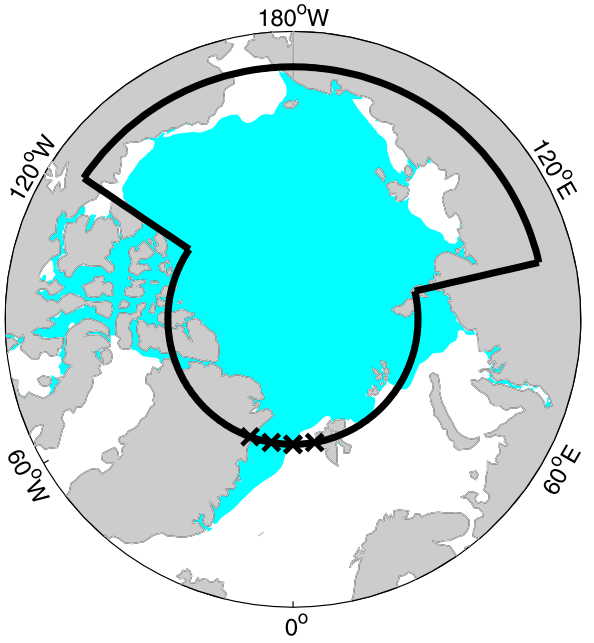

Figure 1. The Arctic domain used in this study. Arctic average drift speed and Arctic average near-surface wind speed are computed over the area bounded by the black curve. See the text for additional details. Crosses mark the portion of the domain boundary that crosses Fram Strait. Cyan shading indicates the region where September mean sea ice concentration exceeds 15%, based on NSIDC passive microwave measurements during 1979–2005.

ERA-Interim has been shown to be effective at capturing wind patterns relevant for observed sea ice drift (Spreen et al., 2011; Wettstein & Deser, 2014). For these data, we use monthly mean wind speed (which is an archived variable) as well as monthly mean wind velocity components. Annual averages are computed with respect to the calendar year, rather than the October–September "sea ice year" that is sometimes adopted (e.g., Wettstein & Deser, 2014). We estimate uncertainty in trends following the approach of Santer et al. (2008).

For calculating Arctic average drift speed and wind speed, the averaging domain is the area within the black boundary shown in Figure 1. This is the area north of 68°N for longitudes east of 103°E and west of 124°W and the area north of 79°N at all other longitudes. We chose this domain because it encloses most of the regions with year-round sea ice cover, as indicated by the observed September mean sea ice extent (cyan shading). Our domain is similar to that used by Langehaug et al. (2013), except that it excludes the Kara Sea, where most of the sea ice cover is seasonal. IABP measurements sample almost all of this domain, except that they miss most of the Laptev Sea and a significant portion of the East Siberian Sea (see Rampal et al., 2009, Figure 1). For point measurements (i.e., for IABP data), Arctic averages drift speed is computed using all measurements that fall within the domain in Figure 1. For each gridded data set (i.e., for each model, satellite, or reanalysis product), Arctic averages are computed using all grid points that fall within the domain in Figure 1, using the native grid of the data set.

Following Rampal et al. (2011), when computing Arctic average drift speed, we exclude grid points in the domain that are within 150 km of a coastline. This facilitates comparison with Rampal et al. (2011), and focuses our attention on drifting sea ice rather than landfast ice. This also mitigates some of the effect of poor sampling in the Laptev and East Siberian Seas in the IABP measurements when comparing these data to climate model output. Including grid points near coastlines produces Arctic average drift speeds that are about a factor of two lower.

Models are not consistent regarding what value they assign for sea ice drift velocity in ice free regions. In some models, the sea ice drift velocity is masked in regions where sea ice is absent, whereas in other models the drift velocity is set to zero in ice-free regions. To compute Arctic-average drift speed consistently across models, we sample only gridpoints where sea ice concentration is greater than zero. This also allows for more consistent comparison between models and IABP measurements, since buoys are placed only in locations where sea ice is present.

The distinction between vector "velocity" and scalar "speed" is important in this study. Unless otherwise noted, we will use "sea ice drift" to refer to sea ice drift speed, and when discussing velocity components, we will state that explicitly. Sea ice drift speed, s_i, is not archived for CMIP5 models, and so we compute it from the drift velocity components, u_i and v_i, using the Euclidean norm,

$$s_i = \sqrt{u_i^2 + v_i^2}. \tag{1}$$

On a spherical polar grid, u_i is the eastward drift component, and v_i is the northward drift component. For computational efficiency, one might be tempted to use monthly means of u_i and v_i to compute s_i. That is, one might assume

$$\bar{s}_i \approx \sqrt{\bar{u}_i^2 + \bar{v}_i^2}, \tag{2}$$

where overbar indicates a monthly average. However, if there are submonthly variations in the sign of u_i or v_i, then $\bar{s}_i$ and $\sqrt{\bar{u}_i^2 + \bar{v}_i^2}$ may be very different from each other.

Figure 2 illustrates this temporal sampling effect using data from HadGEM2-CC. During the first 30 days in Figure 2, there are submonthly variations in drift velocity that contribute significantly to the monthly

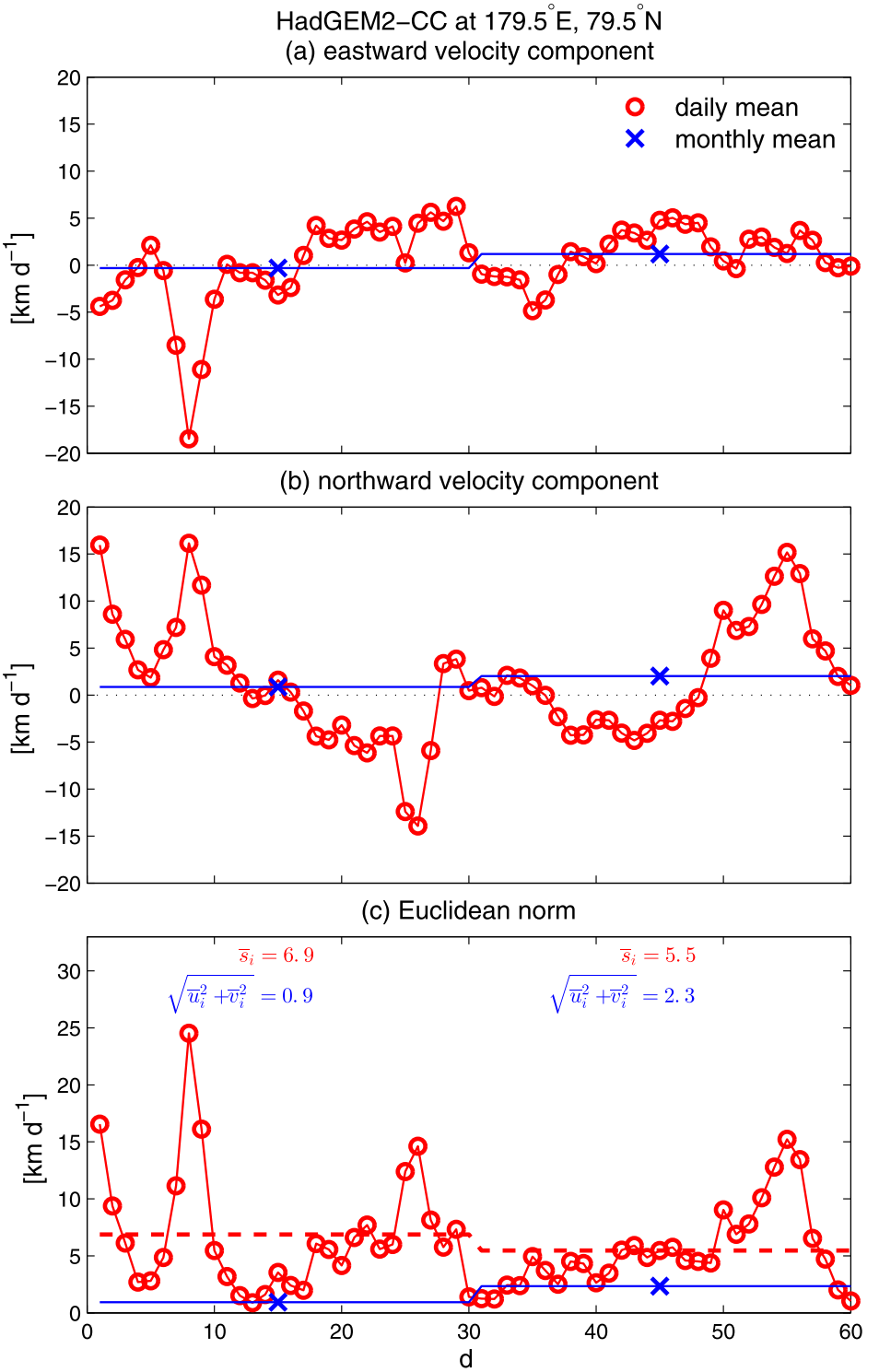

Figure 2. An illustration of the effect of temporal sampling on the computation of drift speed. (a) The eastward component of daily mean (red circles) and monthly mean (blue crosses) sea ice drift velocity at 179.5°E, 79.5°N in HadGEM2-CC during the first 60 days of 1950. (HadGEM2-CC uses a calendar in which every month is 30 days long.) (b) As in Figure 2a but for the northward component of sea ice drift velocity. (c) The Euclidean norms of the daily mean drift velocity (red circles) and the monthly mean drift velocity (blue crosses). Because of submonthly variations in drift direction, the monthly average of the daily mean Euclidean norm (dashed red, $\overline{s}_i$) is a more accurate calculation of sea ice drift speed, and it is substantially greater than the Euclidean norm of the monthly average velocity ($\sqrt{\overline{u}_i^2 + \overline{v}_i^2}$).

average drift speed, and $\bar{s}_i$=6.9 km d^{-1}. Because of strong cancellation between northwestward drift in the first half of the month and southeastward drift in the second half of the month, the monthly means of the eastward and northward velocity components are nearly zero. Thus, $\bar{s}_i$ is almost 8 times greater than $\sqrt{\bar{u}_i^2+\bar{v}_i^2}$ during the first month of the time series. During the second month, the submonthly variability in drift direction is not as strong as during the first month, but it is strong enough that $\bar{s}_i$ and $\sqrt{\bar{u}_i^2+\bar{v}_i^2}$ differ by approximately a factor of two.

If there were no submonthly variations in drift direction, then $\bar{s}_i$ and $\sqrt{\bar{u}_i^2+\bar{v}_i^2}$ would be identical. On the other hand, if submonthly variations in drift direction cancel perfectly so that the monthly average velocity components are zero, then the ratio of $\bar{s}_i$ to $\sqrt{\bar{u}_i^2+\bar{v}_i^2}$ would be infinite. Sea ice drift direction typically varies on timescales of 5 days (Colony & Thorndike, 1984; Rampal et al., 2009), corresponding to the characteristic timescale of synoptic weather systems. Therefore, an accurate computation of sea ice drift speed requires using velocity components sampled on timescales shorter than 5 days. For this reason, we have chosen to compute sea ice drift speed using daily mean velocity components. We will show below that the choice of temporal sampling requires particular attention when comparing models and observations. When computing climatologies and trends of sea ice drift velocity (rather than drift speed), this temporal sampling effect is not relevant, and so we use monthly mean velocity components for these purposes.

As with sea ice drift speed, near-surface wind speed is not archived for the CMIP5 models, and so we compute it from the Euclidean norm of the wind velocity components. We have found that consistent temporal sampling is important when comparing model and observed near-surface wind speed. Thus, for all CMIP5 models, we compute near-surface wind speed from daily mean velocity components. As mentioned above, for ERA-Interim, near-surface wind speed is an archived variable, so it does not need to be computed from velocity components.

3. Evaluation of Model Drift Speed

How well do models reproduce observed sea ice drift speed? Figure 3 shows the seasonal cycle of Arctic average sea ice drift speed. Observations indicate that drift speed (solid curve) is maximum in September–October, when sea ice is thinnest, and it is minimum in March–April, when sea ice is thickest. As Olason and Notz (2014) emphasize, the seasonal cycle of sea ice drift is not driven by the seasonal cycle of near-surface wind, which is maximum in December and minimum in July (dashed curve). A number of models reproduce this basic behavior (e.g., CMCC-CESM and GFDL-CM3), but other models show sea ice drift speeds that are more in phase with near-surface winds (e.g., ACCESS1.3 and MIROC-ESM). Two models (BCC-CSM1.1(m) and CanESM2) produce near-surface wind maxima that appear to lead the maxima of sea ice drift speed. Olason and Notz (2014) and Docquier et al. (2017) have performed observational analysis examining the relationships between the seasonal cycles of drift speed, sea ice concentration, and sea ice thickness. We have performed computations (not shown) demonstrating that most models qualitatively reproduce the observed relationships shown in Olason and Notz (2014) and Docquier et al. (2017).

As mentioned in section 2, our choice of temporal sampling is important for the comparison between models and observations. Computing drift speed from monthly mean components (i.e., $\sqrt{\bar{u}_i^2+\bar{v}_i^2}$), produces drift speeds that are about a factor of two lower than in Figure 3 (not shown). Docquier et al. (2017) have shown a similar effect of temporal sampling on the computation of sea ice drift speed in one particular model. In some models, temporal sampling also affects the apparent timing of the seasonal peak of sea ice drift speed. For example, in the GFDL models, the peak drift speed occurs in September, in agreement with observations (Figure 3). However, when monthly mean velocity components are used, there is no September peak in sea ice drift speed (not shown). Rampal et al. (2011) computed sea ice drift speed from models participating in phase 3 of the Coupled Model Intercomparison Project (CMIP3) using monthly mean velocity components and compared it to buoy drift speed computed from daily mean velocity components. This inconsistency in temporal sampling likely explains much of the apparent disagreement between models and observations in that study. We will revisit this matter in more detail below.

Even when daily temporal sampling is used, there are large intermodel differences in climatological mean sea ice drift speed. For example, CMCC-CESM produces mean sea ice drift speed that is about half that of MPI-ESM-LR and about a third of that in INM-CM4, even though surface wind speeds in these three models are comparable. Figure 4 shows maps of 1979–2005 annual mean sea ice drift and near-surface wind in

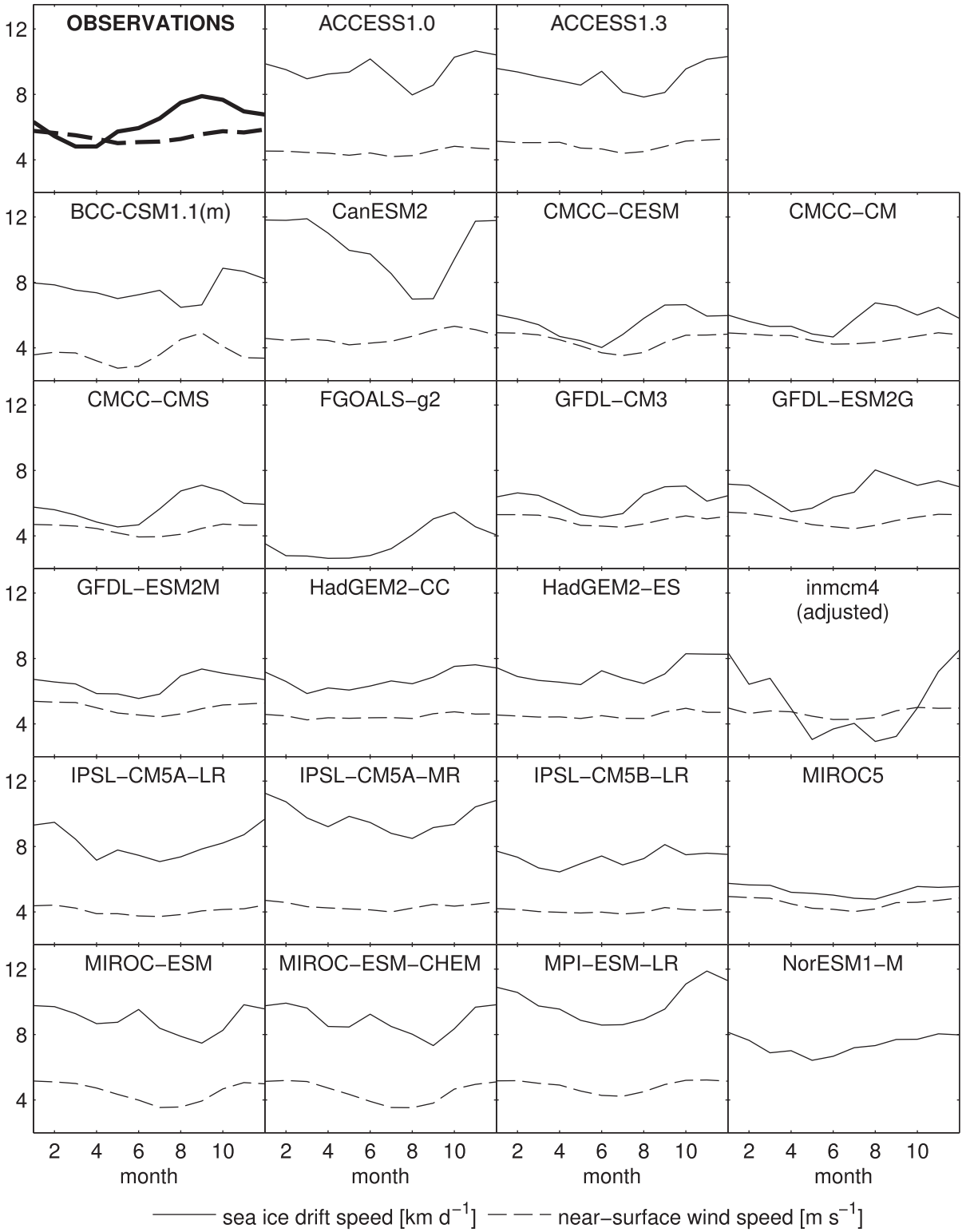

Figure 3. Seasonal cycle of (solid) Arctic average drift speed and (dashed) near-surface wind speed for the period 1979–2005. Arctic averages are computed as detailed in section 2. The vertical scale is km d^{-1} for sea ice drift speed and m s^{-1} for near-surface wind speed. For models with multiple realizations, only the first realization is shown. Drift speed in INM-CM4 is unrealistically high, and so for plotting purposes, we have shifted it down by 10 km d^{-1}. The FGOALS-g2 and NorESM1-M models did not provide the daily wind velocity data needed to accurately compute near-surface wind speed.

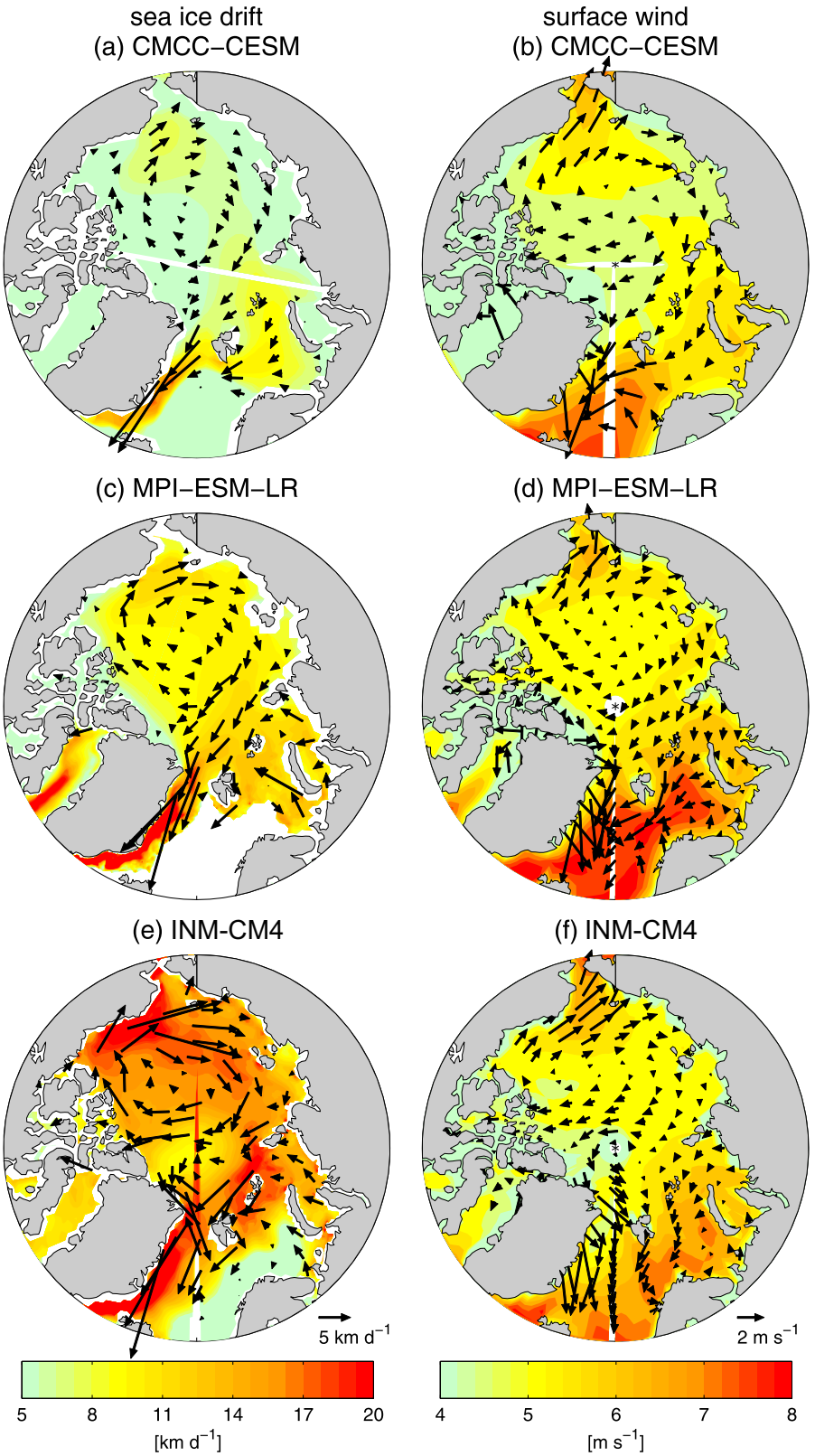

Figure 4. (left column) 1979–2005 average of sea ice drift speed (shading) and velocity (vectors) for (a) CMCC-CESM, (c) MPI-ESM-LR and (e) INM-CM4. (right column) As in the left column for near-surface wind speed (shading) and velocity (vectors). Regions where data are missing are colored white. Note that because of the nonlinearity of computing speed (see section 2 and Figure 2), the length of a vector may not equal the average speed at a given location.

these models. All three models produce qualitatively similar patterns of sea ice motion, including the Beaufort Gyre and transpolar drift patterns seen in observations (Kwok, 2011). (Kwok [2011] has already performed a detailed comparison of regional sea ice drift in models and observations, and so here we focus on the intermodel spread in climatological sea ice drift. Also note that there is an apparent singularity in the INM-CM4 sea ice drift output near the Prime Meridian; see Figure 4e. We have tested masking this singularity, and this had no noticeable effect on calculations of Arctic average drift speed.) In Figure 4, the intermodel differences in sea ice drift speed are distributed throughout the Arctic, and they are not accounted for in a simple way by differences in near-surface wind speed and direction. This suggests that differences in model parameters are likely responsible for much of the intermodel scatter in climatological sea ice drift speed.

Table 2, as introduced in section 2, provides key parameters that likely influence climatological drift speed in climate models. The strength parameter (P^*) and the ice-ocean drag coefficient (C_{dw}) in INM-CM4 are very close to the values used in FGOALS-g2, CanESM2, and the CMCC models, but the air-ice drag coefficient (C_{da}) in INM-CM4 is greater by a factor of 2–2.5. This likely explains why climatological sea ice drift speed in INM-CM4 is so much greater. The values of P^* and C_{da} in all three MIROC models are identical, but the value of C_{dw} in MIROC5 is 4 times greater than that in MIROC-ESM and MIROC-ESM-CHEM. This likely explains why drift speed in MIROC5 is lower than in MIROC-ESM and MIROC-ESM-CHEM. Accounting for drift speed differences among other models is difficult because those models differ in multiple model parameters that are relevant for sea ice drift speed, and there are also differences in turbulence parameterizations for determining air-ice drag. One might also expect climatological sea ice thickness to influence climatological drift speed, but we did not find a clear association between these quantities.

Figure 5a shows the long-term evolution of sea ice drift speed. The observed annual mean drift speed (thick red line) is ~5.5 km d^{-1} in 1979, increasing to ~7.5 km d^{-1} in 2015. Most of the models quantitatively agree with or exceed the observed 1979–2015 mean. About half of the models produce long-term positive trends in sea ice drift speed between 1970 and 2050. Most of the models show decreasing drift speed after 2050. We compare model and observed trends more quantitatively below.

As with the computation of the seasonal cycle, consistent temporal sampling is important when comparing model drift speed time series with observations. Figure5b shows that when model drift speed is computed from monthly mean velocity components, it is about a factor of two lower than the drift speed computed from daily mean velocity components (Figure 5a), and almost all models appear to underestimate observed drift speed. As mentioned above, Rampal et al. (2011) computed model drift speed time series from monthly mean velocity components and compared them to drift speed computed from daily IABP measurements (see their Figure 3), and this produced results similar to our Figure 5b. This suggests that inconsistent temporal sampling was the reason for much of the apparent disagreement between simulated and observed time series in Rampal et al. (2011). Our results show that simulated sea ice drift speed comes into closer agreement with observations when consistent temporal sampling is applied to models and observations.

Figure 6 shows time series of March and September drift speed. Here, we have applied 20 year smoothing to all model time series in order to display their long-term evolution more clearly. Most models produce positive March drift speed trends prior to 2070 (Figure 6a). In contrast, most models produce negative September drift speed trends (Figure 6b), and for the few models that produce positive trends, those trends are weaker than in observations. Altogether, this suggests that, in most models, the long-term evolution of annual mean sea ice drift speed reflects a cancellation between positive trends during winter and negative trends during summer. During March, most models produce unrealistically high climatological drift speed, but most models produce realistic trends. In contrast, during September, most models produce realistic climatological drift speed, but unrealistic long-term trends.

Figure 7 provides a quantitative comparison of sea ice drift speed trends in models and observations during 1979–2015. The annual mean linear trend of the IABP record is 0.65 ± 0.38 km d^{-1} dec^{-1} (Figure 7a). None of the models produce annual mean trends that are as strong as observed, but 17 of the models produce statistically significant positive trends. Seven models produce trends that lie within the range of uncertainty of the observed trend. Most models produce March drift speed trends in agreement with observations (Figure 7b), but none of the models reproduce the strong positive observed trend during September

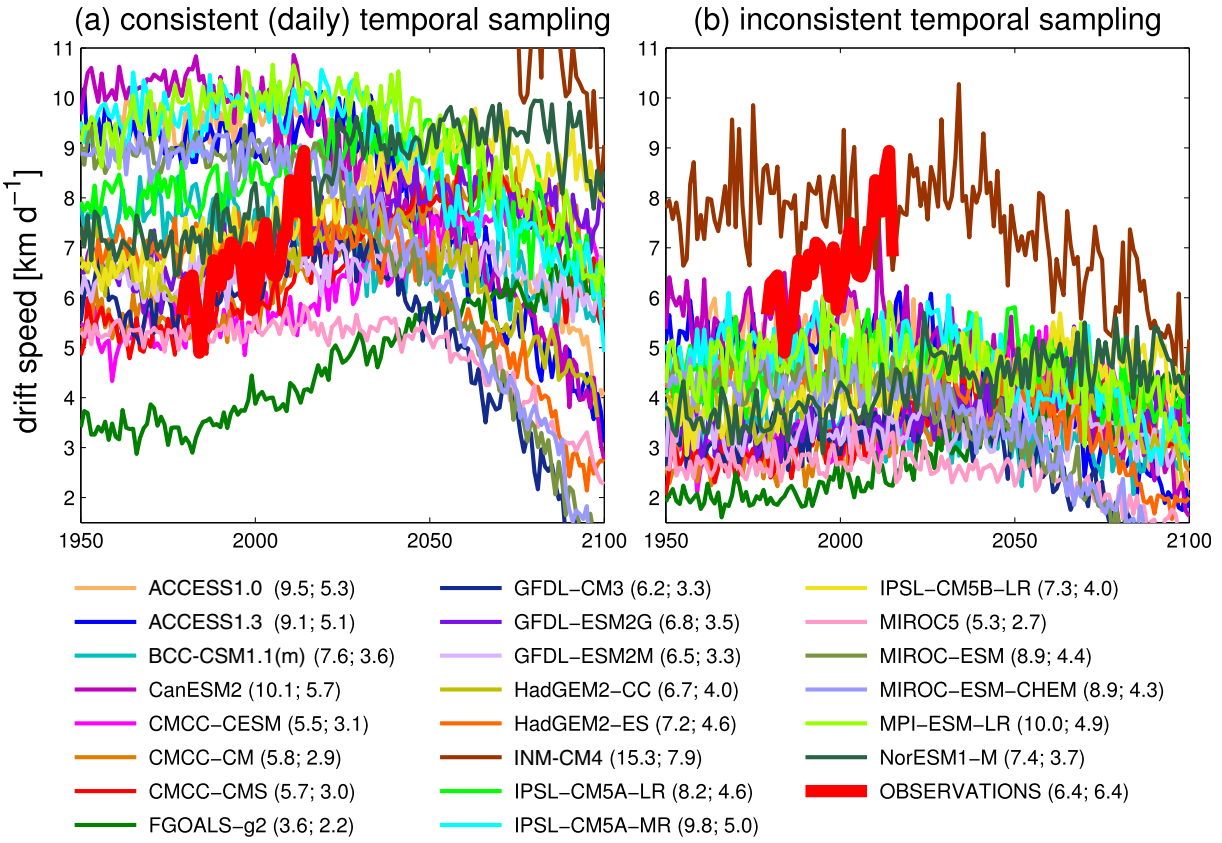

Figure 5. Thin lines show CMIP5 annual mean Arctic average drift speed computed from (a) daily mean velocity components and (b) monthly mean velocity components. For models with multiple realizations, only the first realization is shown. The left plot mostly excludes one outlier model (INM-CM4) with unrealistically high drift speed. The thick red line (identical in both plots) shows annual mean drift speed computed from daily IABP measurements. Next to each name in the legend, we show in parentheses the corresponding 1979–2005 average value of drift speed in Figure 5a (first number) and Figure 5b (second number) in units of km d^{-1}. This facilitates quantitative comparison, as well as the pinpointing of particular curves in the plots.

(Figure 7c). Thus, much of the disagreement between modeled and observed annual mean drift speed trends likely arises because of poor reproduction of the observed summer drift speed trend.

During summer, the uncertainty of the observed drift speed trends is 2–3 times greater than the trend uncertainty in most of the models (Figure 7c). One possible contribution to the different trend uncertainties is that the temporal variability of sea ice drift speed in models differs from that in observations. Another contribution is that there are temporal variations in the locations sampled by the buoys, whereas there are no such spatial sampling variations in the models. Thus, the uncertainty ranges shown in Figure 7 account for the key sources of uncertainty when computing Arctic average drift speed, and this allows for a rigorous comparison between observations and climate models.

Some of the apparent intermodel differences in Figure 7 may be due to differences in model physics, and some might be due to internal climate variability. To address this, we have analyzed initial condition ensembles of MIROC5 (five ensemble members, pink circles in Figure 7) and IPSL-CM5A-LR (four ensemble members, green circles). (See section 2 for additional details regarding initial condition ensembles.) The intraensemble spread in MIROC5 and IPSL-CM5A-LR suggest that approximately half of the apparent intermodel spread in March drift speed trends may be due to internal variability. Internal variability accounts for approximately a third of the apparent intermodel spread in September and annual mean drift speed trends.

4. Drivers of Long-Term Trends During Winter

Our analysis above shows that there is a strong contrast between winter Arctic average drift speed trends (which are positive in most models and in good agreement with observations) and summer trends (which

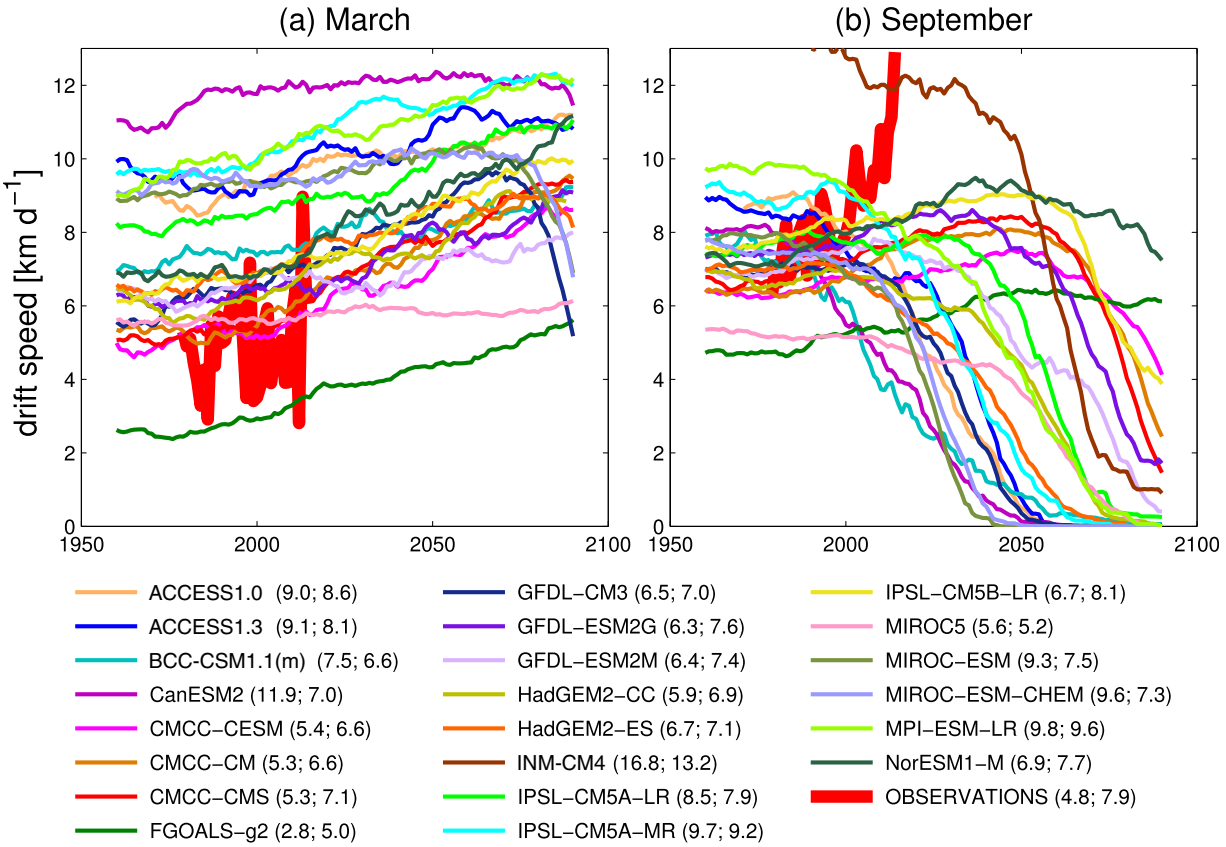

Figure 6. (a) The thick red line shows March Arctic average drift speed from IABP measurements. Thin lines show March Arctic average drift speed for the CMIP5 models. For clarity, 20 year smoothing has been applied to the CMIP5 time series. (b) As in Figure 6a for September means. Figure 6a excludes the outlier INM-CM4 model. Next to each name in the legend, we show in parentheses the corresponding 1979–2005 average value of March drift speed (first number) and September drift speed (second number) in units of km d^{-1}.

are negative in most models and in poor agreement with observations). Thus, to understand the long-term evolution of model drift speed, we must understand the contrasting physical mechanisms at work during the winter and summer seasons. In this section, we analyze in more detail the simulated winter trends to demonstrate that the physical mechanisms driving these trends indeed reflect mechanisms at work in the real world.

To highlight one model, Figure 8a shows the regional structure of March sea ice drift trends in GFDL-CM3. There are positive drift speed trends throughout the Arctic, with weaker positive trends northeast of Greenland compared to elsewhere. This contrasts with long-term trends of near-surface wind speed (Figure 8b), which are positive over Fram Strait and along the Russian coast and negative over the central Arctic. These wind speed changes appear to drive sea ice drift speed trends in specific regions (such as along the eastern coast of Greenland), but neither wind speed nor wind direction changes explain the positive trend of sea ice drift speed in the central Arctic. We have also examined changes in the ocean circulation near the surface (not shown), and while these appear to modulate sea ice drift trends in particular regions they do not explain the increase in sea ice drift speed throughout the Arctic.

It is more likely that the widespread drift speed increase is driven primarily by the widespread reduction in sea ice thickness (Figure 8c). The sea ice thinning is greatest in regions where the sea ice is historically thickest, as expected from the growth rate feedback discussed by Bitz and Roe (2004) and Holland et al. (2008). This sea ice thinning leads to a reduction in sea ice strength, which reduces the sea ice internal stress, allowing for more sea ice deformation, more fracturing, and faster drift. Evidence for such a physical mechanism has been shown in models (Docquier et al., 2017) and observations (Rampal et al., 2009; Spreen et al., 2011).

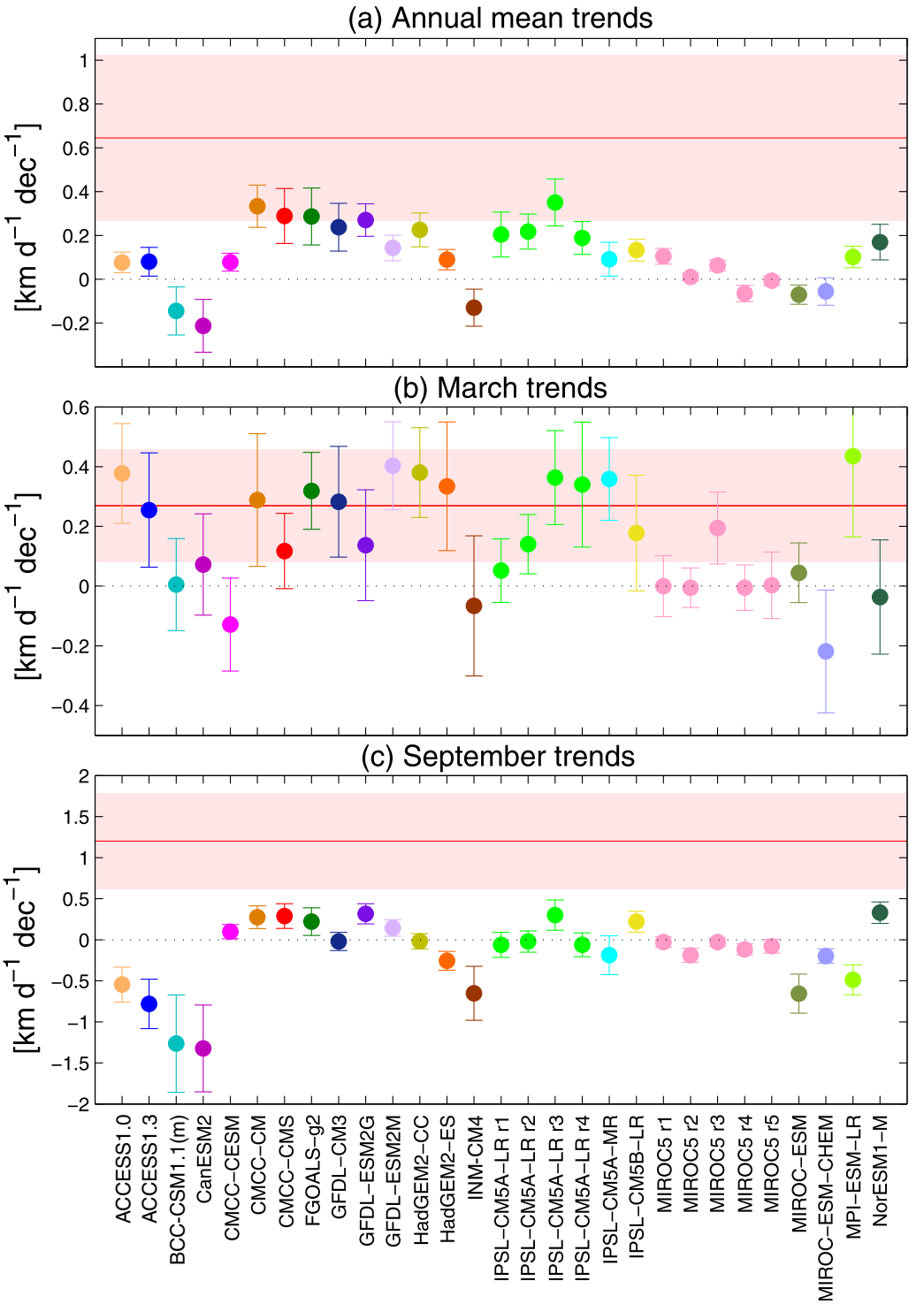

Figure 7. (a) 1979–2015 linear trends of Arctic average annual mean drift speed in each of the CMIP5 runs. Error bars indicate the trend uncertainty, computed following Santer et al. (2008). The red line indicates the trend computed from IABP measurements, with the range of trend uncertainty indicated in light red. (b) As in Figure 7a but for March drift speed. (c) As in Figure 7a but for September drift speed.

In GFDL-CM3, the trend of sea ice thickness is approximately -0.3 m dec^{-1} in the Western Arctic, and the drift speed trend is approximately 0.7 km d^{-1} dec^{-1} in this region. This is quantitatively comparable to expectations based on the historical relationship between sea ice drift speed and thickness in the seasonal

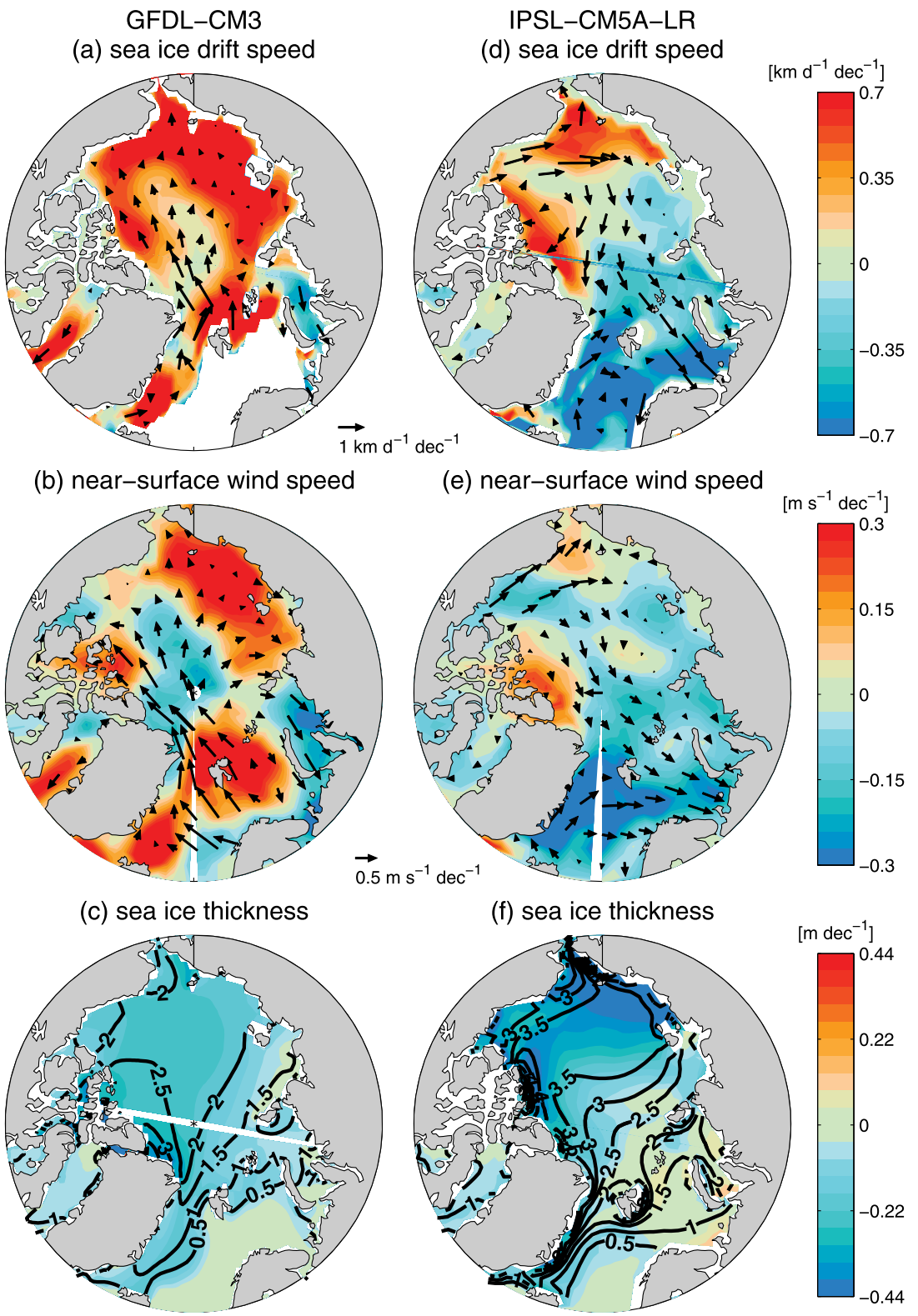

Figure 8. (a) 1979–2015 linear trends of March sea ice drift speed (shading) and velocity (vectors) in GFDL-CM3. (b) As in Figure 8a for near-surface wind speed (shading) and velocity (vectors). (c) 1979–2015 linear trend (shading) and 1979–2005 climatology (contours in units of m) of March sea ice thickness in GFDL-CM3. (d–f) As in Figures 8a–8c for the first realization of IPSL-CM5A-LR. Regions where data are missing are colored white.

cycles of models and observations. (E.g., note the slopes of the red and black dashed lines in Figure 4b of Docquier et al., 2017.)

We arrive at a similar explanation for the sea ice drift trends in IPSL-CM5A-LR (Figure 8d). Changes in near-surface winds drive drift speed trends in particular regions like Fram Strait (Figure 8e), and changes in the ocean circulation appear to modulate drift speed trends in parts of the Beaufort Sea (not shown), but the widespread positive trend in sea ice drift speed elsewhere in the Arctic is more closely associated with the Arctic-wide reduction of sea ice thickness (Figure 8f). Interestingly, IPSL-CM5A-LR shows a wind-driven decrease in drift speed in Fram Strait, in contrast to the positive drift speed trend elsewhere in the Arctic. That is, in this model, the dominant driver of drift speed change in Fram Strait (near-surface wind) is clearly distinct from the dominant driver of drift speed change elsewhere in the Arctic (sea ice thinning).

Such a distinction is also apparent in observations. Sea ice drift through Fram Strait is primarily wind driven (Kwok et al., 2004; Smedsrud et al., 2011). Trends in both Fram Strait outflow and near-surface wind over Fram Strait have been positive since 1957 (Smedsrud et al., 2011, 2017). However, since 1979 there has been no significant positive trend in Arctic-average near-surface wind speed, and so the positive trend in Arctic-average sea ice drift speed during this time is likely due to sea ice thinning (Rampal et al., 2009; Spreen et al., 2011). Furthermore, satellite observations show that wintertime trends in Fram Strait drift speed were negative during 1992–2009 (corresponding to negative trends in near-surface wind speed), in contrast to the positive drift speed trends elsewhere in the Arctic (driven by sea ice thinning) (Spreen et al., 2009, Figure 1). Thus, an increase in Arctic average drift speed does not necessarily imply an increase in Fram Strait outflow. In other words, without knowledge of wind forcing changes, one cannot assume that there is a change in Fram Strait outflow because there is a change in Arctic-average drift speed.

These claims are further supported by results from other CMIP5 models. Figure 9 shows the multimodel mean trends of March 1979–2015 sea ice drift, near-surface wind, and sea ice thickness. Included in this multimodel average are nine of the models that produced statistically significant positive trends of March drift speed, all of which agree with buoy observations (Figure 7b). These models are ACCESS1.0, ACCESS1.3, CMCC-CM, GFDL-CM3, GFDL-ESM2M, HadGEM2-CC, HadGEM2-ES, IPSL-CM5A-LR, and IPSL-CM5A-MR. IPSL-CM5A-LR was ensemble averaged prior to taking the multimodel mean. MIROC5 was excluded from the multimodel mean since most of its ensemble members did not produce significant positive trends. FGOALS-g2 was not included in the multimodel mean since daily near-surface wind velocity was not available for this model. Model trends were remapped to a spherical polar grid using nearest neighbor interpolation prior to taking the multimodel mean.

The multimodel mean sea ice drift speed trends are positive over most of the Arctic Ocean (Figure 9a). In particular regions, these drift speed trends are modulated by near-surface wind speed trends (Figure 9b) and ocean current speed trends (not shown), but the primary driver of the large-scale drift speed trend is the widespread sea ice thinning (Figure 9c). Furthermore, the multimodel mean shows decreasing March drift speed in Fram Strait, in contrast to the positive drift speed trend elsewhere in the Arctic. (As mentioned above, such a contrast is plausible, given the contrasting trends shown in satellite observations; see Spreen et al., 2011.) Thus, in agreement with observations, most climate models exhibit widespread positive trends in winter Arctic average sea ice drift speed that are primarily driven by sea ice thinning.

5. Drivers of Long-Term Trends During Summer

The analysis of section 3 showed that CMIP5 models produce weakly positive or negative trends of September Arctic average drift speed during 1979–2005. For the models that produce positive summer drift speed trends, these trends are primarily associated with long-term sea ice thinning (not shown), as was the case for March drift speed trends. But why do none of the models produce drift speed trends as strong as observed? Why do most models produce negative September drift speed trends?

One possibility is that some physical mechanisms responsible for summer sea ice drift are misrepresented in climate models. Figure 10 shows the regional structure of observed September drift speed (shading) and

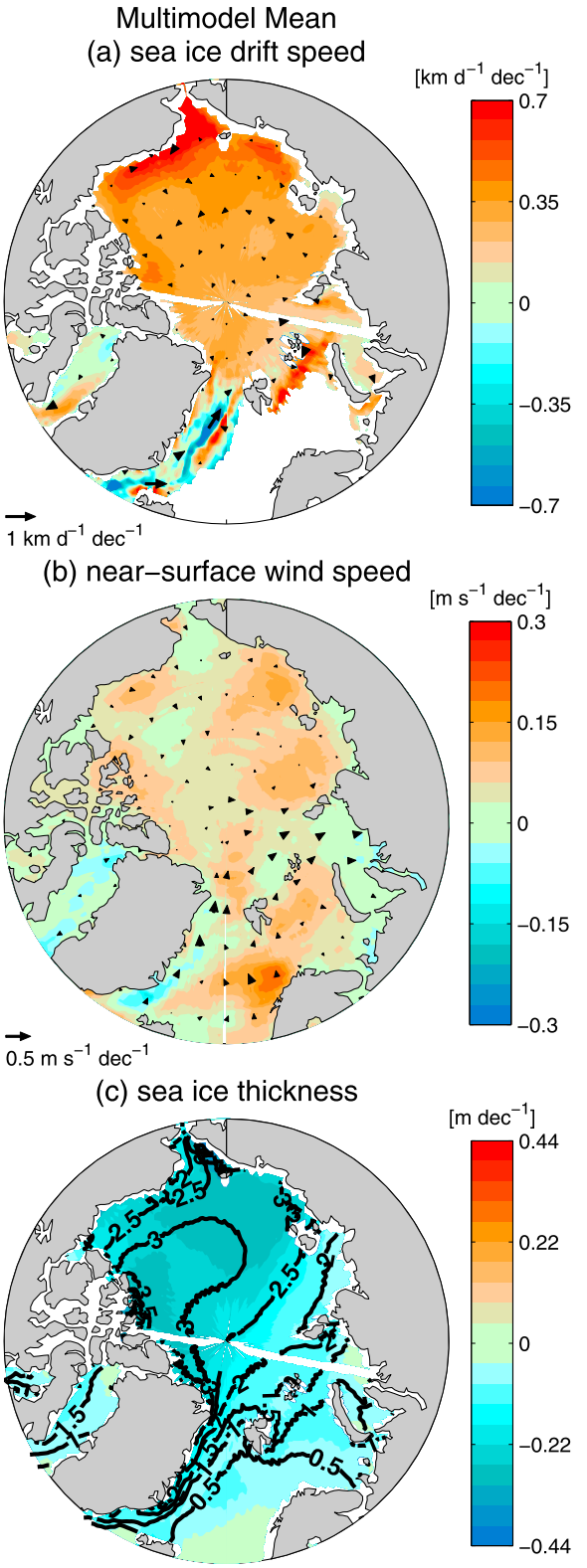

Figure 9. As in Figure 8 for the multimodel mean computed from nine of the models that produce statistically significant positive trends of March 1979–2015 Arctic average sea ice drift speed, in agreement with buoy observations. See the text for additional details about which models were included in the multimodel mean.

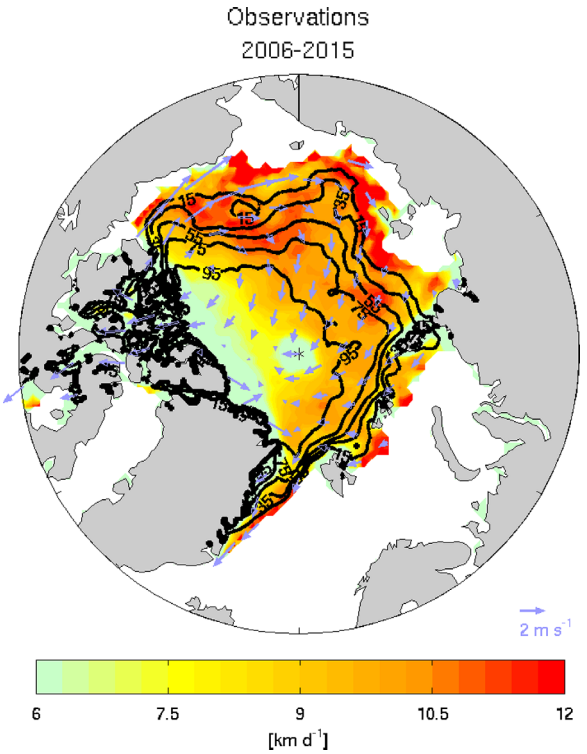

Figure 10. 2006–2015 September sea ice drift speed from the Kimura satellite measurements (shading), sea ice concentration from passive microwave measurements (black contours), and near-surface wind velocity from ERA-Interim reanalysis (vectors). The lowest sea ice concentration contour is 15% and the contour interval is 20%. For clarity, wind vectors are omitted in regions where sea ice concentration is less than 1%. Regions where sea ice drift data are missing are colored white.

sea ice concentration (contours) from satellite-based measurements averaged over 2006–2015. (See section 2 for additional details about these data.) In agreement with the physical mechanisms discussed earlier, this shows that regions of less concentrated (typically thinner) sea ice exhibit faster drift speed, with near-surface winds (vectors) acting as a modulating influence.

CMCC-CM and GFDL-ESM2M both show characteristics similar to observations during 2006–2015 (Figure 11, top row): drift speed is enhanced in regions of less concentrated sea ice. Because of internal variability, we would not expect a precise correspondence between modeled and observed fields during 2006–2015. Nonetheless, the negative correspondence between sea ice concentration and drift speed is clear in both models and observations during this period. However, in CMCC-CM during later periods, when sea ice covers a smaller portion of the Arctic Ocean, there is evidence of the opposite association: drift is slower in regions of less concentrated sea ice (Figures 11b and 11c). There is some strengthening of near-surface wind in regions of less concentrated sea ice, but this has little apparent influence on sea ice drift speed. The relationship between sea ice drift and concentration is more complex in GFDL-CM3: in the late 21st century, there is evidence of lower drift speed in regions of less concentrated sea ice, but this appears to be offset by stronger winds in some regions of less concentrated sea ice (Figures 11e and 11f). We reach the same conclusions when examining the relationship between sea ice drift speed and sea ice thickness, but we focus here on sea ice concentration to facilitate comparison between models and observations.

The other CMIP5 models exhibit qualitatively similar behavior (not shown): as the Arctic Ocean transitions from full to partial sea ice cover, the relationship between sea ice drift speed and strength changes. When the Arctic is fully ice-covered, simulated sea ice concentration and sea ice drift speed show a negative correlation (as in observations), but as the Arctic becomes partially ice-covered, this correlation weakens and (in most models) changes sign. In some models, such as BCC-CSM1.1(m) (Figure 12), the Arctic is partially ice-covered during summer for the entire period after 2005. In these models, the correlation between sea ice drift speed and strength is negative throughout this period. This apparent "sea ice extent effect" is likely responsible for the weakly positive or negative simulated trends of summer sea ice drift speed.

The causes of the sea ice extent effect in models are not clear. One possibility is that sea ice interaction with surrounding sea ice and coastal boundaries is contributing significantly to sea ice deformation (and hence drift speed) in models, and as the sea ice extent decreases, these contributions to sea ice deformation weaken. More work is needed to investigate the causes of the sea ice extent effect in detail. We have also considered the possibility that increases in low-level stability are reducing the air-ice drag and thus contributing to long-term decreases in September drift speed. However, most of the CMIP5 models produce decreases in September low-level stability over the 21st century (not shown), and so this does not explain the long-term decrease in September drift speed in most models.

During winter, the Arctic is fully ice covered in all models for almost the entire 1950–2100 period, and the models consistently show realistic negative correlations between sea ice drift speed and strength (not shown). Thus, there is essentially no contribution of the sea ice extent effect to simulated winter drift speed trends, and sea ice thinning is the dominant driver of long-term positive trends of sea ice drift speed. This further establishes that the degree to which the Arctic is fully ice covered is highly consequential for simulated sea ice drift speed trends. It is possible that this sea ice extent effect is stronger in models than in observations, and this would explain why September drift speed trends are lower in models than in observations. Continued satellite observations of summer sea ice drift will help to substantiate this and remedy possible model deficiencies.

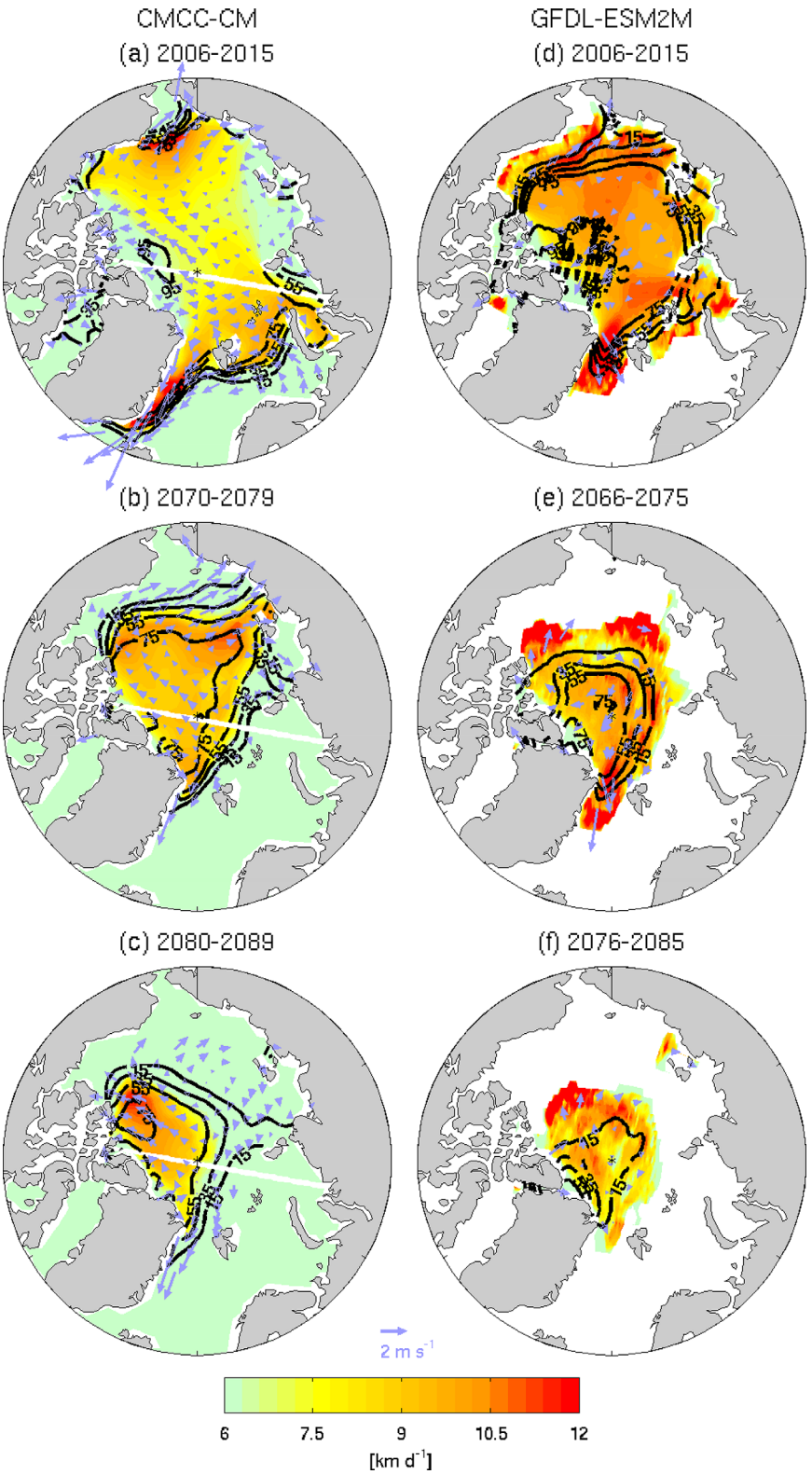

Figure 11. As in Figure 10 for (left column) CMCC-CM and (right column) GFDL-ESM2M during three 10 year periods. (top row) The 2006–2015 period, which overlaps with available observations, and (middle and bottom rows) the two decades prior to the Arctic becoming nearly ice free. In this context, the Arctic is considered "nearly ice free" when the 20 year running average of September sea ice area falls below 0.3×10^{12} m^2, where sea ice area is computed over the domain shown in Figure 1.

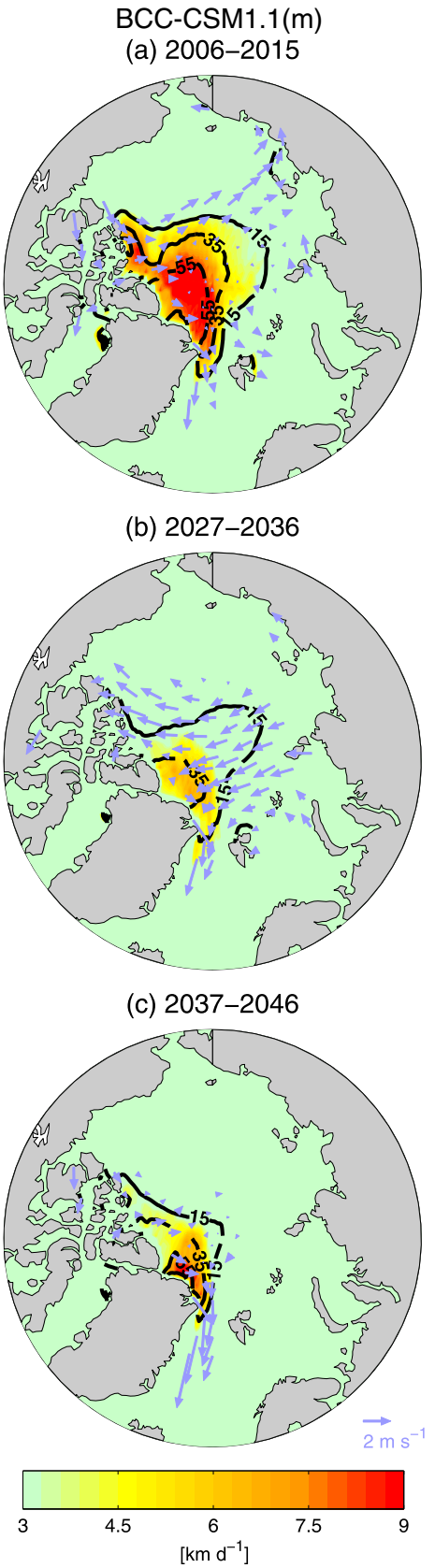

Figure 12. As in Figure 11 for BCC-CSM1.1(m). For clarity, the shading scale is different from that in Figures 10 and 11.

6. Summary and Conclusions

The key conclusion of this study is that model simulations of sea ice drift are more realistic than suggested by Rampal et al. (2011). Consistent temporal sampling is crucial when comparing sea ice drift speed in models and observations. About half of the CMIP5 models analyzed in this study exhibit positive long-term trends of annual mean sea ice drift speed during 1979–2015, and almost all models exhibit negative trends in annual mean sea ice drift speed in the late 21st century. The simulated annual mean trends reflect strong cancellation between winter trends, which are positive in most models and in good agreement with observations, and summer trends, which are negative in most models and in poor agreement with observations.

Even when consistent temporal sampling is applied, there is considerable intermodel scatter in climatological sea ice drift speed. Intermodel differences in prescribed parameters (e.g., the ice-ocean drag coefficient and sea ice surface roughness length) explain much of this scatter. Altogether, our study helps to highlight aspects in which models show agreement with observations, while pinpointing aspects in which models require improvement. This provides valuable information that will help modeling centers improve model performance and model projections.

Long-term increasing trends in simulated March Arctic average drift speed are driven primarily by sea ice thinning, and this relationship is clear when examining individual models as well as the mean of models with realistic historical trends. Thus, model evidence provides support for the existence of a "drift acceleration feedback" (Rampal et al., 2011), although more work is needed to determine if drift acceleration acts to accelerate or decelerate Arctic sea ice loss. Models suggest that a positive trend of Arctic average drift speed does not necessarily imply a positive trend of sea ice outflow at Fram Strait. The latter is primarily influenced by trends in near-surface wind speed, which are not necessarily positive (cf., Spreen et al., 2011).

During summer, as the Arctic transitions from full to partial sea ice cover, the simulated relationship between sea ice drift speed and strength changes dramatically. This sea ice extent effect likely explains the disagreement between simulated and observed trends of summer sea ice drift speed. However, more work is needed to explain the cause of the sea ice extent effect in models and determine whether this effect is at all relevant in the real world. Continued observations of regional sea ice drift and continued archiving of daily sea ice drift velocity from models will greatly facilitate such work.

Acknowledgments

Funding for this work has been provided primarily by the Canadian Sea Ice and Snow Evolution (CanSISE) Network. NFT acknowledges a Bjerknes Visiting Fellowship from the Bjerknes Centre for Climate Research for stimulating his collaboration with J.J.W. and C.L. D.D. is funded by the European Commission's Horizon 2020 PRIMAVERA program (641727). J.J.W. and C.L. are partially supported by project DynAMiTe (255027) funded by the Research Council of Norway. Noriaki Kimura kindly provided the daily satellite-based measurements of summer sea ice drift velocity. We acknowledge the modeling centers for participating in CMIP5 and for providing helpful responses to our inquiries about the sea ice models. We thank Dave Bailey for helpful discussions, and we thank the editor Andrey Proshutinsky and the anonymous reviewers for their constructive feedback. All data used in this study are properly cited with details provided in the list of references.

References

Bi, D., M., Dix, S. J., Marsland, S., O'Farrell, H., Rashid, P., Uotila, A., et al. (2013). The ACCESS coupled model: Description, control climate and evaluation. *Australian Meteorological and Oceanographic Journal*, *63*, 41–64.

Bitz, C. M., & Roe, G. H. (2004). A mechanism for the high rate of sea ice thinning in the Arctic Ocean. *Journal of Climate*, *17*, 3623–3632. https://doi.org/10.1175/1520-0442(2004)017<3623:AMFTHR>2.0.CO;2

Colony, R., & Thorndike, A. S. (1984). An estimate of the mean field of Arctic sea ice motion. *Journal of Geophysical Research*, *89*, 10,623–10,629. https://doi.org/10.1029/JC089iC06p10623

Comiso, J. C., Parkinson, C. L., Gersten, R., & Stock, L. (2008). Accelerated decline in the Arctic sea ice cover. *Geophysical Research Letters*, *35*, L01703. https://doi.org/10.1029/2007GL031972

Dee, D. P., Uppala, S. M., Simmons, A. J., Berrisford, P., Poli, P., Kobayashi, S., et al. (2011). The ERA-Interim reanalysis: Configuration and performance of the data assimilation system. *Quarterly Journal of the Royal Meteorological Society*, *137*, 553–597. https://doi.org/10.1002/qj.828

Delworth, T. L., Broccoli, A. J., Rosati, A., Stouffer, R. J., Balaji, V., Beesley, J. A., et al. (2006). GFDL's CM2 global coupled climate models. Part I: Formulation and simulation characteristics. *Journal of Climate*, *19*, 643–674. https://doi.org/10.1175/JCLI3629.1

Deser, C., Walsh, J. E., & Timlin, M. S. (2000). Arctic sea ice variability in the context of recent atmospheric circulation trends. *Journal of Climate*, *13*, 617–633. https://doi.org/10.1175/1520-0442(2000)013<0617:ASIVIT>2.0.CO;2

Ding, Q., Schweiger, A., L'Heureux, M., Battisti, D. S., Po-Chedley, S., Johnson, N. C., et al. (2017). Influence of high-latitude atmospheric circulation changes on summertime Arctic sea ice. *Nature Climate Change*, *7*, 289–295. https://doi.org/10.1038/nclimate3241

Docquier, D., Massonnet, F., Barthélemy, A., Tandon, N. F., Lecomte, O., & Fichefet, T. (2017). Relationships between Arctic sea ice drift and strength modelled by NEMO-LIM3.6. *Cryosphere*, *11*, 2829–2846. https://doi.org/10.5194/tc-11-2829-2017

Flato, G. M., & Hibler, W. D. (1992). Modeling pack ice as a cavitating fluid. *Journal of Physical Oceanography*, *22*, 626–651. https://doi.org/10.1175/1520-0485(1992)022<0626:MPIAAC>2.0.CO;2

Gorodetskaya, I. V., Tremblay, L.-B., Liepert, B., Cane, M. A., & Cullather, R. I. (2008). The influence of cloud and surface properties on the Arctic Ocean shortwave radiation budget in coupled models. *Journal of Climate*, *21*, 866–882. https://doi.org/10.1175/2007JCLI1614.1

Haas, C., Pfaffling, A., Hendricks, S., Rabenstein, L., Etienne, J.-L., & Rigor, I. (2008). Reduced ice thickness in Arctic transpolar drift favors rapid ice retreat. *Geophysical Research Letters*, *35*, L17501. https://doi.org/10.1029/2008GL034457

Hibler, W. D. (1979). A dynamic thermodynamic sea ice model. *Journal of Physical Oceanography*, *9*, 815–846. https://doi.org/10.1175/1520-0485(1979)009<0815:ADTSIM>2.0.CO;2

Holland, M. M., Bailey, D. A., Briegleb, B. P., Light, B., & Hunke, E. (2012). Improved sea ice shortwave radiation physics in CCSM4: The impact of melt ponds and aerosols on Arctic sea ice. *Journal of Climate*, *25*, 1413–1430. https://doi.org/10.1175/JCLI-D-11-00078.1

Holland, M. M., Serreze, M. C., & Stroeve, J. (2008). The sea ice mass budget of the Arctic and its future change as simulated by coupled climate models. *Climate Dynamics*, *34*, 185–200. https://doi.org/10.1007/s00382-008-0493-4

Hunke, E. C., & Dukowicz, J. K. (1997). An elastic-viscous-plastic model for sea ice dynamics. *Journal of Physical Oceanography*, *27*, 1849–1867. https://doi.org/10.1175/1520-0485(1997)027<1849:AEVPMF>2.0.CO;2

Hunke, E. C., Lipscomb, W. H., Turner, A. K., Jeffery, N., & Elliott, S. (2015). CICE: The Los Alamos sea ice model documentation and software user's manual (Tech. Rep. LA-CC-06–012). Los Alamos, NM: Los Alamos National Laboratory.

Kimura, N., Nishimura, A., Tanaka, Y., & Yamaguchi, H. (2013). Influence of winter sea-ice motion on summer ice cover in the Arctic. *Polar Research*, *32*, 20193. https://doi.org/10.3402/polar.v32i0.20193

Komuro, Y., Suzuki, T., Sakamoto, T. T., Hasumi, H., Ishii, M., Watanabe, M., et al. (2012). Sea-ice in twentieth-century simulations by new MIROC coupled models: A comparison between models with high resolution and with ice thickness distribution. *Journal of the Meteorological Society of Japan*, *90A*, 213–232. https://doi.org/10.2151/jmsj.2012-A11

Kwok, R. (2011). Observational assessment of Arctic Ocean sea ice motion, export, and thickness in CMIP3 climate simulations. *Journal of Geophysical Research*, *116*, C00D05. https://doi.org/10.1029/2011JC007004

Kwok, R., Cunningham, G. F., & Pang, S. S. (2004). Fram Strait sea ice outflow. *Journal of Geophysical Research*, *109*, C01009. https://doi.org/10.1029/2003JC001785

Langehaug, H., Geyer, F., Smedsrud, L., & Gao, Y. (2013). Arctic sea ice decline and ice export in the CMIP5 historical simulations. *Ocean Modelling*, *71*, 114–126. https://doi.org/10.1016/j.ocemod.2012.12.006

Lu, Y., Zhou, M., & Wu, T. (2013). Validation of parameterizations for the surface turbulent fluxes over sea ice with CHINARE 2010 and SHEBA data. *Polar Research*, *32*, 20818. https://doi.org/10.3402/polar.v32i0.20818

Maslowski, W., Marble, D., Walczowski, W., Schauer, U., Clement, J. L., & Semtner, A. J. (2004). On climatological mass, heat, and salt transports through the Barents Sea and Fram Strait from a pan-Arctic coupled ice-ocean model simulation. *Journal of Geophysical Research*, *109*, C03032. https://doi.org/10.1029/2001JC001039

McLaren, A. J., Banks, H. T., Durman, C. F., Gregory, J. M., Johns, T. C., Keen, A. B., et al. (2006). Evaluation of the sea ice simulation in a new coupled atmosphere-ocean climate model (HadGEM1). *Journal of Geophysical Research*, *111*, C12014. https://doi.org/10.1029/2005JC003033

Meier, F., W., Fetterer, M., Savoie, S., Mallory, R. D., & Stroeve, J. (2013). *NOAA/NSIDC climate data record of passive microwave sea ice concentration* (version 2). Boulder, Colorado USA. NSIDC: National Snow and Ice Data Center. https://doi.org/10.7265/N55M63M1.

Notz, D. (2012). Challenges in simulating sea ice in earth system models. *Wiley Interdisciplinary Reviews: Climate Change*, *3*, 509–526. https://doi.org/10.1002/wcc.189

Notz, D., & Stroeve, J. (2016). Observed Arctic sea-ice loss directly follows anthropogenic CO_2 emission. *Science*, *354*, 747–750. https://doi.org/10.1126/science.aag2345

Olason, E., & Notz, D. (2014). Drivers of variability in Arctic sea-ice drift speed. *Journal of Geophysical Research: Oceans*, *119*, 5755–5775. https://doi.org/10.1002/2014JC009897

Rampal, P., Weiss, J., Dubois, C., & Campin, J.-M. (2011). IPCC climate models do not capture Arctic sea ice drift acceleration: Consequences in terms of projected sea ice thinning and decline. *Journal of Geophysical Research*, *116*, C00D07. https://doi.org/10.1029/2011JC007110

Rampal, P., Weiss, J., & Marsan, D. (2009). Positive trend in the mean speed and deformation rate of Arctic sea ice, 1979–2007. *Journal of Geophysical Research*, *114*, C05013. https://doi.org/10.1029/2008JC005066

Rigor, I. G., Wallace, J. M., & Colony, R. L. (2002). Response of sea ice to the Arctic oscillation. *Journal of Climate*, *15*, 2648–2663. https://doi.org/10.1175/1520-0442(2002)015<2648:ROSITT>2.0.CO;2

Rothrock, D. A. (1975). The energetics of the plastic deformation of pack ice by ridging. *Journal of Geophysical Research*, *80*, 4514–4519. https://doi.org/10.1029/JC080i033p04514

Santer, B. D., Thorne, P. W., Haimberger, L., Taylor, K. E., Wigley, T. M. L., Lanzante, J. R., et al. (2008). Consistency of modelled and observed temperature trends in the tropical troposphere. *International Journal of Climatology*, *28*, 1703–1722. https://doi.org/10.1002/joc.1756

Screen, J. A., Simmonds, I., & Keay, K. (2011). Dramatic interannual changes of perennial Arctic sea ice linked to abnormal summer storm activity. *Journal of Geophysical Research*, *116*, D15105. https://doi.org/10.1029/2011JD015847

Serreze, M. C., Holland, M. M., & Stroeve, J. (2007). Perspectives on the Arctic's shrinking sea-ice cover. *Science*, *315*, 1533–1536. https://doi.org/10.1126/science.1139426

Serreze, M. C., Stroeve, J., Barrett, A. P., & Boisvert, L. N. (2016). Summer atmospheric circulation anomalies over the Arctic Ocean and their influences on September sea ice extent: A cautionary tale. *Journal of Geophysical Research: Atmospheres*, *121*, 11,463–11,485. https://doi.org/10.1002/2016JD025161

Smedsrud, L. H., Halvorsen, M. H., Stroeve, J. C., Zhang, R., & Kloster, K. (2017). Fram Strait sea ice export variability and September Arctic sea ice extent over the last 80 years. *Cryosphere*, *11*, 65–79. https://doi.org/10.5194/tc-11-65-2017

Smedsrud, L. H., Sirevaag, A., Kloster, K., Sorteberg, A., & Sandven, S. (2011). Recent wind driven high sea ice area export in the Fram Strait contributes to Arctic sea ice decline. *Cryosphere*, *5*, 821–829. https://doi.org/10.5194/tc-5-821-2011

Spreen, G., Kern, S., Stammer, D., & Hansen, E. (2009). Fram Strait sea ice volume export estimated between 2003 and 2008 from satellite data. *Geophysical Research Letters*, *36*, L19502. https://doi.org/10.1029/2009GL039591

Spreen, G., Kwok, R., & Menemenlis, D. (2011). Trends in Arctic sea ice drift and role of wind forcing: 1992–2009. *Geophysical Research Letters*, *38*, L19501. https://doi.org/10.1029/2011GL048970

Stroeve, J., Holland, M. M., Meier, W., Scambos, T., & Serreze, M. (2007). Arctic sea ice decline: Faster than forecast. *Geophysical Research Letters*, *34*, L09501. https://doi.org/10.1029/2007GL029703

Stroeve, J., & Notz, D. (2015). Insights on past and future sea-ice evolution from combining observations and models. *Global and Planetary Change*, *135*, 119–132. https://doi.org/10.1016/j.gloplacha.2015.10.011

Stroeve, J. C., Kattsov, V., Barrett, A., Serreze, M., Pavlova, T., Holland, M., et al. (2012b). Trends in Arctic sea ice extent from CMIP5, CMIP3 and observations. *Geophysical Research Letters*, *39*, L16502. https://doi.org/10.1029/2012GL052676

Stroeve, J. C., Serreze, M. C., Holland, M. M., Kay, J. E., Malanik, J., & Barrett, A. P. (2012a). The Arctic's rapidly shrinking sea ice cover: A research synthesis. *Climatic Change*, *110*, 1005–1027. https://doi.org/10.1007/s10584-011-0101-1

Sumata, H., Kwok, R., Gerdes, R., Kauker, F., & Karcher, M. (2015). Uncertainty of Arctic summer ice drift assessed by high-resolution SAR data. *Journal of Geophysical Research: Oceans*, *120*, 5285–5301. https://doi.org/10.1002/2015JC010810

Taylor, K. E., Stouffer, R. J., & Meehl, G. A. (2012). An overview of CMIP5 and the experiment design. *Bulletin of the American Meteorological Society*, *93*, 485–498. https://doi.org/10.1175/BAMS-D-11-00094.1

Tschudi, M., Fowler, C., Maslanik, J., Stewart, J. S., & Meier, W. (2016). *Polar Pathfinder daily 25 km EASE-grid sea ice motion vectors* (version 3). Boulder, CO: National Snow and Ice Data Center. https://doi.org/10.5067/O57VAIT2AYYY

Vancoppenolle, M., Fichefet, T., Goosse, H., Bouillon, S., Madec, G., & Maqueda, M. A. M. (2009). Simulating the mass balance and salinity of Arctic and Antarctic sea ice. 1. Model description and validation. *Ocean Modelling*, *27*, 33–53. https://doi.org/10.1016/j.ocemod.2008.10.005

Wang, M., & Overland, J. E. (2009). A sea ice free summer Arctic within 30 years? *Geophysical Research Letters*, *36*, L07502. https://doi.org/10.1029/2009GL037820, l07502

Wettstein, J. J., & Deser, C. (2014). Internal variability in projections of twenty-first-century Arctic sea ice loss: Role of the large-scale atmospheric circulation. *Journal of Climate*, *27*, 527–550. https://doi.org/10.1175/JCLI-D-12-00839.1

Williams, J., Tremblay, B., Newton, R., & Allard, R. (2016). Dynamic preconditioning of the minimum September sea-ice extent. *Journal of Climate*, *29*, 5879–5891. https://doi.org/10.1175/JCLI-D-15-0515.1

Winton, M. (2011). Do climate models underestimate the sensitivity of Northern Hemisphere sea ice cover? *Journal of Climate*, *24*, 3924–3934. https://doi.org/10.1175/2011JCLI4146.1

Yakovlev, N. G. (2003). Coupled model of ocean general circulation and sea ice evolution in the Arctic Ocean. *Izvestiya, Atmospheric and Oceanic Physics*, *39*, 355–368.